



Article

Production of Permanent Magnets from Recycled NdFeB Powder with Powder Extrusion Moulding

Stefan Rathfelder ¹, Stephan Schuschnigg ², Christian Kukla ^{2,*}, Clemens Holzer ² and Carlo Burkhardt ^{1,*}

¹ Institute for Precious and Technology Metals, Pforzheim University, Tiefenbronner Str. 65, 75175 Pforzheim, Germany; stefan.rathfelder@hs-pforzheim.de

² Department of Polymer Engineering and Science, Institute of Polymer Processing, Montanuniversitaet Leoben, Otto Gloeckel-Straße 2, 8700 Leoben, Austria; stephan.schuschnigg@unileoben.ac.at (S.S.); clemens.holzer@unileoben.ac.at (C.H.)

* Correspondence: christian.kukla@unileoben.ac.at (C.K.); carlo.burkhardt@hs-pforzheim.de (C.B.); Tel.: +43-3842-402-8403 (C.K.); +49-7231-28-6063 (C.B.)

Abstract: In the last fifteen years, several groups have investigated metal injection moulding (MIM) of NdFeB powder to produce isotropic or anisotropic rare earth magnets of greater geometric complexity than that achieved by the conventional pressing and sintering approach. However, due to the powder's high affinity for oxygen and carbon uptake, sufficient remanence and coercivity remains difficult. This article presents a novel approach to producing NdFeB magnets from recycled material using Powder Extrusion Moulding (PEM) in a continuous process. The process route uses powder obtained from recycling rare earth magnets through Hydrogen Processing of Magnetic Scrap (HPMS). This article presents the results of tailored powder processing, the production of mouldable feedstock based on a special binder system, and moulding with PEM to produce green and sintered parts. The magnetic properties and microstructures of debinded and sintered samples are presented and discussed, focusing on the influence of filling ratio and challenging processing conditions on interstitial content as well as density and magnetic properties.

Keywords: powder extrusion moulding (PEM); metal injection moulding (MIM); production of NdFeB permanent magnets; recycling of EOL-magnets



Citation: Rathfelder, S.; Schuschnigg, S.; Kukla, C.; Holzer, C.; Burkhardt, C. Production of Permanent Magnets from Recycled NdFeB Powder with Powder Extrusion Moulding. *J. Manuf. Mater. Process.* **2024**, *8*, 81. <https://doi.org/10.3390/jmmp8020081>

Academic Editor: Steven Y. Liang

Received: 27 February 2024

Revised: 11 April 2024

Accepted: 15 April 2024

Published: 18 April 2024



Copyright: © 2024 by the authors. Licensee MDPI, Basel, Switzerland. This article is an open access article distributed under the terms and conditions of the Creative Commons Attribution (CC BY) license (<https://creativecommons.org/licenses/by/4.0/>).

1. Introduction

Considering the annual demand for electrical appliances, electric cars, and even wind turbines, rare earths such as neodymium or dysprosium are key industrial materials in Europe and worldwide. The mobility sector, in particular, is expected to see a sharp increase in demand. The shift from internal combustion engines to electric drives has created considerable demand for Nd-Fe-B magnets. Given that 95% of today's electric cars use Rare Earth Permanent Magnets (REPMs), demand will increase from 5000 t/year in 2019 to 70,000 t/year in 2030. Demand for wind turbines is also expected to increase five to six times by 2030 [1]. Every year, 16,000 tonnes of rare earth magnets are exported from China to Europe, accounting for around 98% of the European market [2]; thus, Europe heavily depends on China. In addition, rare earth magnet mining damages the environment and causes disease due to groundwater contamination [2].

To overcome these challenges, the EU-funded SUSMAGRPO project is attempting to locate, sort, and produce new permanent magnets from end-of-life magnets [3].

This article introduces a novel technique for manufacturing NdFeB permanent magnets using powder extrusion moulding (PEM). As the demand for these magnets is expected to increase in the next few years, the PEM process is a potential manufacturing method. Producing permanent magnets in large quantities with a finished final contour is possible with this process. This process eliminates the need for time-consuming post-processing of sintered parts, such as grinding.

NdFeB magnets can be differentiated according to their production type. A distinction can be made between (a) sintered magnets, (b) bonded magnets, and (c) MIM (Metal Injection Moulding) magnets [4,5]. Sintered magnets are produced by the classical powder metallurgy process. The powder is poured into a mould while a magnetic field is applied, causing the magnetic particles to align in their preferred magnetocrystalline direction (c-axis), parallel to the field lines. Pressing maintains the magnetic orientation of the particles. The next stage involves sintering the components in a vacuum or inert gas environment [6,7]. Sintered magnets are typically formed into blocks and require machining through various cutting processes, such as wire cutting or surface grinding, to achieve their final shape. By contrast, MIM or PEM magnets require almost no post-processing, as the final shape is produced directly. During sintering, the magnetic particles lose their orientation as the Curie temperature of NdFeB is exceeded. NdFeB's Curie temperature ranges from 310 °C to 400 °C, depending on its composition. To reorient the magnetic domains after sintering, the sintered part is remagnetised using an external magnetic field [7]. Sintered NdFeB magnets have the highest energy products than other types of magnets [8].

Unlike sintered magnets, polymer-bonded magnets require a polymer binder system. The magnetic powder is mixed with the binder in a mixer or extruder. However, the correct powder/binder ratio must be considered. Reducing the binder amount can positively affect magnetic properties but negatively affect mechanical properties. Polymer-bonded magnets can be produced by injection moulding, extrusion, compression moulding, or additive manufacturing [4,9,10]. Another method of manufacturing NdFeB permanent magnets is the MIM process. This process combines the advantages of sintered and polymer-bonded magnets and is suitable for the mass production of components with complex and precise geometries [11]. For MIM magnets' magnetic properties to perform as well as sintered magnets, the binder must be removed from the green parts. Once the binder has been removed, the components are sintered in a furnace to create a metallic structure [4].

The objective of this study was to create a procedure for manufacturing NdFeB-based isotropic permanent magnets using the Powder Extrusion Moulding (PEM) technique. The main difference between MIM and PEM processes is the different shapes of parts. Compared with MIM, the starting material in the PEM process is pressed continuously and slowly through an uncooled nozzle, producing a continuous strand with precise cross-sectional dimensions. Both processes have four steps, as seen in Figure 1.

Firstly, the feedstock is compounded into a blend of finely ground powder and a binder system consisting of polymers. The binder coats the powder and ensures good flowability of the feedstock. Typically, a binder system comprises three components: the main binder, the backbone binder, and the additives. The main binder ensures that the melted feedstock has good flow properties and holds the green part together. The backbone binder ensures that the brown part remains cohesive after eliminating the main binder. Additives facilitate wetting of the metal powder by the binder and prevent agglomeration [6,12].

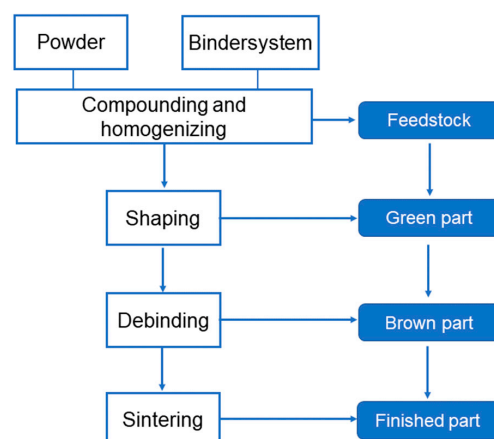


Figure 1. Process steps MIM/PEM, according to [13].

One of the challenges of MIM/PEM is to identify an appropriate powder-to-binder proportion. High binder content can cause segregation or excessive shrinkage, while high powder content can increase viscosity and cause incomplete cavity filling. Powder content typically ranges between 50 vol% and 60 vol% by volume. Powder content below 50 vol% reduces the probability of creating a densely sintered component [12,13]. Compounding the feedstock homogeneously for further production is important, as previously described. Depending on the application, tumblers are used for mixing, and kneaders or twin-screw extruders are used for materials with high shear input [13,14].

In the MIM process, the binder is melted, allowing the feedstock to be injected with high pressure into a cooled cavity using an injection moulding machine and enabling the creation of intricate geometries. The MIM process is generally well-explained in the literature [6,11,12], particularly for NdFeB permanent magnet production [15–17]. The result is the so-called green part. As per research conducted by Gonzalez-Gutierrez et al. [18] and Sotomayor et al. [19], the PEM process combines powder metallurgy and polymer extrusion. In the PEM process, the binder is also melted in the extruder. However, unlike MIM, the feedstock is continuously and slowly pressed through an uncooled nozzle to produce an endless strand with precise cross-sectional dimensions. Sotomayor et al. [19] conducted an experiment producing thin 430 L stainless steel tubes with PEM. They investigated the impact of torque on homogeneity during mixing and filling, which increased torque until it stabilised shortly thereafter. When the torque reached a steady point, the feedstock was deemed homogeneously mixed. Furthermore, the team noted that a raised powder load leads to increased torque. In their study examining profile production from tool steel via extrusion, Gonzalez-Gutierrez et al. [18] evaluated the dimensional stability of extruded profiles with different filling degrees. The feedstock consisted of particles ranging from 10 to 45 microns, which were blended in a twin-screw extruder and then granulated. The profiles were extruded using a single-screw extruder and cooled with air at the die before being withdrawn at a uniform speed of 100 mm/s. Their study findings showed that profiles with 60 vol% filler contents displayed the best dimensional stability. The researchers also described the effects of excessively high haul-off speeds on extrudate thickness. If the speed was too high, the extrudates thinned out, as demonstrated by samples extruded with 50 vol% and 60 vol% powders. It can be inferred that profiles with 60 vol% powder filling exhibit better dimensional stability than profiles with 50 vol% and 55 vol% powder fillings.

Once the components have been shaped, the binder has fulfilled its purpose and must be eliminated. Usually, a binder system consists of a main binder and a backbone binder; in these cases, a multi-stage debinding process is applied. In the first step, the main binder is removed. Depending on the binder, it can be removed thermally with a solvent or catalytically. Typically, the main binder is removed with a solvent or catalytically. These processes remove the main binder from the outside inwards, creating an open-pored structure held together only by the backbone binder, from which the main binder is removed. The disadvantage of thermally debinding the main binder is that the binder evaporates without a clear exit route, leading to cracks in the component as the temperature rises. To avoid this, a very low heat rate is selected, which can make the debinding process very time-consuming. The backbone binder is thermally removed from the sintering furnace prior to sintering. Debinding parameters such as heat rate, debinding time, and temperature are adapted to the part. Debinded parts are called brown parts [20].

The final processing step is sintering. In a thermal treatment (typically about 80% of the material's melt temperature), the brown part is transformed into a dense, mechanically loadable, solid part. Due to their high surface energy, the particles fuse together through diffusion and cratering processes. The gas atmosphere, temperature, and heating/cooling rates for sintering NdFeB must be adjusted according to furnace equipment and material composition. Davies et al. provide a detailed description of the sintering behaviour of NdFeB [21]. They carried out sintering tests on green parts of Nd₁₆Fe₇₆B₈ magnets produced by isostatic pressing. The samples were sintered at temperatures between 600 °C and 1100 °C. They showed that a temperature of 655 °C caused the material density to

increase because the Nd-rich grain boundary phase started to melt. At a temperature of 1100 °C, the density increased to 98% of the theoretical maximum. In ideal cases, MIM parts with a theoretical density of 99.5% can be produced [13].

A prerequisite for producing anisotropic NdFeB magnets is the avoidance of impurities such as oxygen and carbon. Since the highly reactive Nd-rich phase strongly tends to absorb oxygen, the production process is carried out almost entirely in an argon atmosphere. Initially, the primary binder is eliminated with a solvent. Subsequently, the component is merely held together by the backbone, which undergoes thermal decomposition in the sintering furnace. Burkhardt et al. [22] showed that removing the backbone binder during thermal debinding is a critical step in the process chain, as the Nd-rich phase must be prevented from being contaminated with carbon. If the Nd-rich phase reacts with carbon, it forms Nd carbides, which precipitate α -iron due to loss of stoichiometry and degraded magnetic properties [23]. As Nd hydrides are more stable than Nd carbides, the hydrated powder is assumed to be more stable to carbon impurities than the dehydrated powder. If the oxygen and/or carbon content is too high, liquid phase sintering is inhibited and the sinter density is reduced. Minowa et al. [24] showed that carbon impurities have an even more deleterious effect on magnet coercivity than oxygen. They also [24] determined that oxygen and carbon values increase with each manufacturing step. Kim et al. [25] found that magnet coercivity decreased significantly with high oxygen values. For these reasons, process control during powder preparation, extrusion, thermal debinding, and sintering is crucial for components with good magnetic properties.

2. Experimental

Figure 2 shows the process for producing recycled permanent magnets with PEM through micrographs.

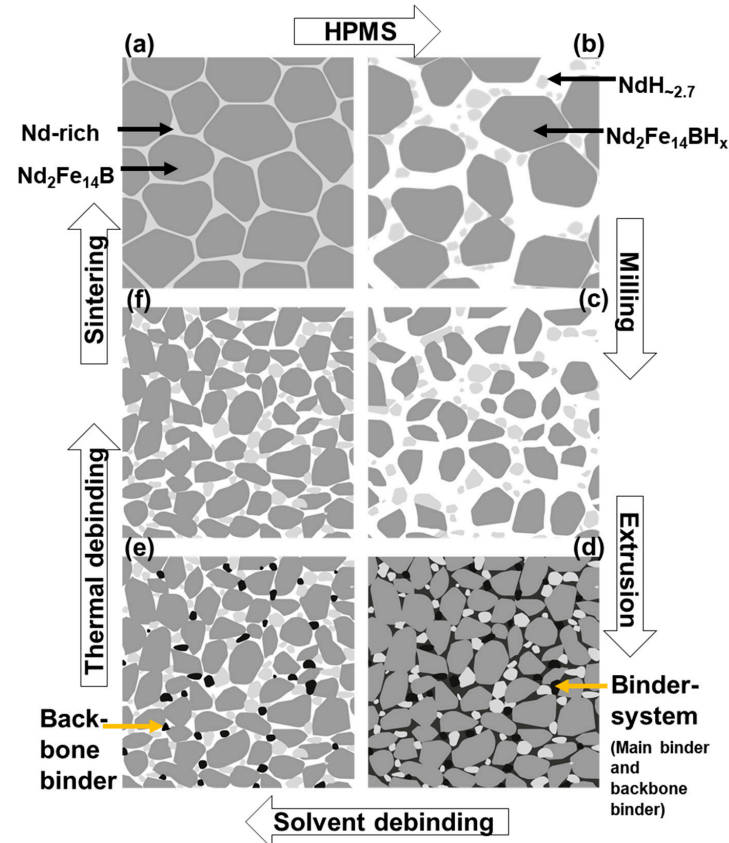


Figure 2. Process flow production of recycled permanent magnets with PEM. (a) microstructure sintered magnet, (b) HPMS-powder, (c) milled powder, (d) powder mixed with binder (e) microstructure after solvent debinding (f) Microstructure after thermal debinding.

2.1. Materials

The raw material used was an end-of-life (EOL) wind turbine magnet. The chemical composition is provided in Table 1.

Table 1. Chemical composition of the starting magnet provided in wt%, ICP-OES.

| Fe | Nd | B | Dy | Pr | Cr | Ni | Si | Ce | Rare Earth |
|-------|-------|------|------|------|------|------|------|--------|------------|
| 64.78 | 27.60 | 0.99 | 4.17 | 0.10 | 0.01 | 0.01 | 0.20 | 0.0129 | 31.90 |

The magnetic values and density of the starting anisotropic magnet are provided in Table 2.

Table 2. Magnetic values and density of the starting anisotropic magnet.

| H_c [kA/m] | B_r [mT] | Density [g/cm ³] |
|--------------|------------|------------------------------|
| 1400 | 1330 | 7.45 |

Figure 3 shows the microstructure of the starting material in an SEM image. The bright areas indicate the Nd-rich phase (A), the dark areas indicate the hard magnetic phase (B), and the black areas are pores (C).

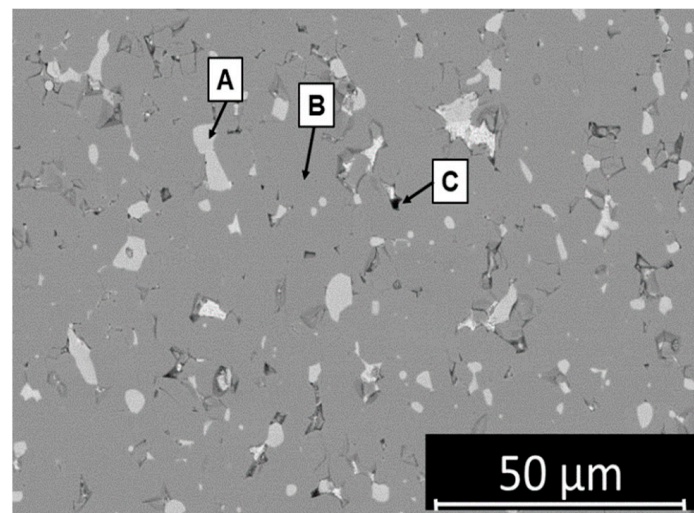


Figure 3. SEM image of the structure of the end-of-life magnet (A) Nd-rich phase, (B) hard-magnetic phase, (C) pores (Note: pores mainly caused by metallographic preparation).

2.1.1. Powder Preparation

There are several methods of recycling REPM. Recycling through hydrometallurgical or pyrometallurgical processes requires significant amounts of energy, water, or chemicals [26]. The HPMS process developed by the University of Birmingham [26] is an eco-friendly and energy-efficient alternative [26,27]. It involves exposing the end-of-life (EOL) magnet to hydrogen in a reactor, which causes the Nd-rich grain boundary phase to hydrogenate and expand. The embrittlement of the grain boundary phase and the expansion of the hard-magnetic phase due to interstitial hydride formation force the grains apart, causing the structure to disintegrate. This process results in a friable, hydrogenated powder consisting of $Nd_2Fe_{14}BH_x$ and $NdH_{-2.7}$ phases, as shown in Figure 2b [28]. The resulting coarse HPMS powder is unsuitable for extrusion as it lacks adequate flow properties. In addition, Zakotnik et al. [29] noted that finely ground powder allows better densification during sintering. Two methods have been established to finely mill HPMS powder: jet milling and ball milling [28,30,31].

In this work, hydrogen was repeatedly added during the HPMS process to keep the pressure constant at 3 bar. This process was repeated until the pressure dropped no further. A Nano 500 MM mixer mill from Retsch GmbH (Haan, Germany) was used to grind the coarse HPMS powder. The powder was ground in three cycles of 10 min at a frequency of 35 Hz. The particle size distribution of the ground powder was measured using a Mastersizer 3000 particle size analyser from Malvern Panalytical GmbH (Nuremberg, Germany), as shown in Table 3.

Table 3. Particle size distribution of ball milled powder.

| Distribution | Powder Size |
|--------------|--------------------|
| Dv(10) | 2.97 μm |
| Dv(50) | 7.68 μm |
| Dv(90) | 16.1 μm |

2.1.2. Binder System

Hartwig et al. [17] showed that binder systems for NdFeB magnet production based on polyoxymethylene (POM) are unsuitable for injection moulding as the raw material quickly decomposes at moulding temperature. Therefore, Burkhardt et al. [22] developed a binder system based on a powder/thermoplastic blend and additives. The binder system consists of a main and backbone binder, as shown in Figure 2d. The main binder coats the NdFeB particles and protects against oxidation so that the fine powder can be processed in the PEM process. In addition, the main binder ensures good feedstock flowability. The backbone binder ensures that the open-pored part does not collapse after solvent debinding, as seen in Figure 2e [13]. Stearic acid is used as an additive so that the particles are more effectively wetted by the polymer. In this study, we used a binder system that provided good flow properties for shaping and cohesion of the brown part, as well as protecting the highly reactive Nd-rich phase.

2.2. Compounding and Extrusion Process

The process of creating NdFeB feedstock for PEM is illustrated in Figure 4.

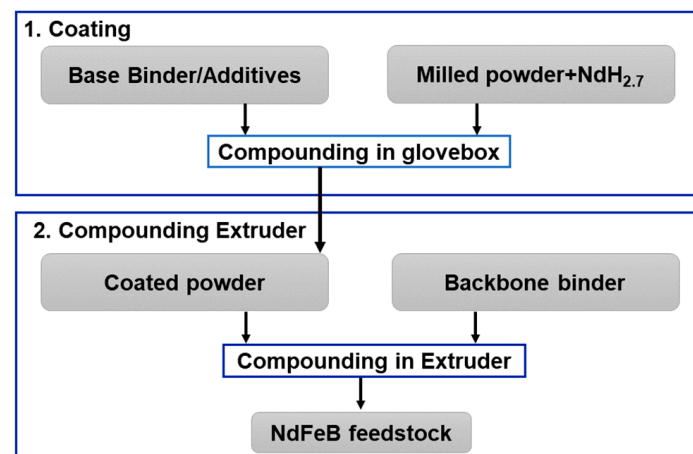


Figure 4. Process for the preparation of NdFeB feedstock.

In the first step of feedstock production, the finely ground powder is coated with the main binder in an argon atmosphere in a glove box. The main binder is dissolved in an organic solvent and mixed with the powder. The resulting mixture is then vacuum-dried for 24 h. The dried feedstock is subsequently crushed into granules in a mortar, ready for further processing in the extruder. Burkhardt et al. [22] noted that the porosity of MIM magnets manufactured from recycled material without the addition of NdH_{2.7} is higher

than recycled MIM magnets with the addition of 2 wt% NdH_{-2.7}. The reason for this is that the oxygen content of recycled NdFeB material typically contains 0.4–0.6 wt%, which is significantly higher than ordinary starting materials at 0.03–0.04 wt%. Mottram et al. [32] showed that the addition of NdH_{-2.7} to the alloy improves coercivity field strength. If too much NdH_{-2.7} is added, the remanence is reduced; therefore, extrusion tests were carried out with 1 wt% NdH_{-2.7} and 3 wt% NdH_{-2.7}. NdH_{-2.7} powder was added to the HPMS powder prior to the coating step. In the feedstock composition, the addition of NdH_{-2.7} was subtracted from the milled HPMS material. Moreover, 1 g of NdH_{-2.7} is added to 99 g of HPMS powder for a feedstock of 100 g powder content and 1 wt% NdH_{-2.7} addition.

In this experiment, different feedstock variants and extrusion parameters were investigated, as shown in Tables 4 and 5. The powder and feedstock for all variants were prepared as described above.

(a) Addition of NdH_{-2.7}

- Feedstock A: 1 wt% NdH_{-2.7} addition;
- Feedstock B: 3 wt% NdH_{-2.7} addition;
- Feedstock C: 3 wt% NdH_{-2.7} addition, non-degassed powder.

As described previously, a feedstock was produced with the addition of 1 wt% and 3 wt% NdH_{-2.7} to investigate any alterations to magnetic values, microstructure, or oxygen values resulting from different NdH_{-2.7} concentrations.

(b) Degassing of the powder HPMS powder

As described in Section 1, conducting experiments with non-degassed and degassed powder is advisable since Nd hydrides have greater stability against carbon impurities during thermal debinding than Nd carbides. Thus, the HPMS powder utilised for feedstocks A and B undergoes a 2 h degassing process at 500 °C within a CarboLite Gero tube furnace in a vacuum.

(c) Powder loading

Samples with 50 vol% and 60 vol% powder loading were extruded. In addition, the behaviour of modified powder loading on the dimensional stability and density of the components was investigated.

(d) Screw speed

Screw speed effects on the feedstock mixture were analysed. The three variants of raw material were processed both at a screw speed of 7 rpm and at a faster screw speed of 15 rpm. The haul-off speed was adapted to the screw speed.

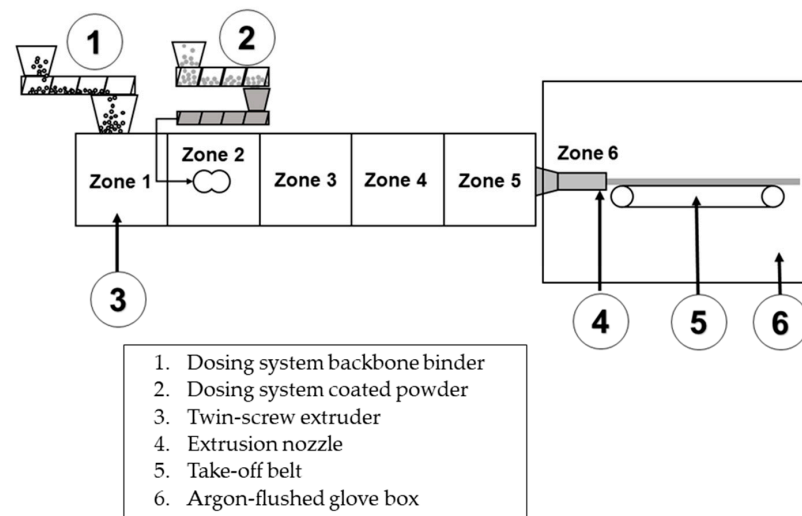
Table 4. Feedstock variants.

| Feedstock | Powder Loading [vol%] | NdH _{2.7} Add. [wt%] | Screw Speed [rpm] | Powder Degassed |
|-----------|-----------------------|-------------------------------|-------------------|-----------------|
| A1 | 60 | 1 | 7 | Yes |
| A2 | 60 | 1 | 15 | Yes |
| A3 | 50 | 1 | 7 | Yes |
| A4 | 50 | 1 | 15 | Yes |
| B1 | 60 | 3 | 7 | Yes |
| B2 | 60 | 3 | 15 | Yes |
| B3 | 50 | 3 | 7 | Yes |
| B4 | 50 | 3 | 15 | Yes |
| C1 | 60 | 3 | 7 | No |
| C2 | 60 | 3 | 15 | No |
| C3 | 50 | 3 | 7 | No |
| C4 | 50 | 3 | 15 | No |

Table 5. Extrusion parameters.

| Extrusion Parameters | Values |
|-----------------------------|--------|
| Temperature Zone 1 [°C] | 80 |
| Temperature Zone 2 [°C] | 150 |
| Temperature Zone 3 [°C] | 155 |
| Temperature Zone 4 [°C] | 155 |
| Temperature Zone 5 [°C] | 155 |
| Temperature Zone 6 [°C] | 160 |
| Screw speed fast [rpm] | 15 |
| Haul-off speed fast [m/min] | 0.2 |
| Screw speed slow [rpm] | 7 |
| Haul-off speed slow [m/min] | 0.1 |

In the second compounding process, the coated powder was blended with the backbone binder in the extruder. For these trials, a co-rotating twin-screw extruder KETSE 12/36 from Brabender GmbH & Co. KG (Duisburg, Germany) with two gravimetric metering units was used. Co-rotating twin-screw extruder technology provides excellent compounding properties and homogeneous compounding of the feedstock. The molten binder and powder were transferred from one screw to the other, resulting in a very homogeneous mixture [33]. The screw configuration involved conveying elements to transport the melt to the nozzle and kneading elements to compound the material. The screws were 12 mm in diameter and 450 mm in length. The schematic extrusion process is shown in Figure 5. After feeders (1) and (2) fed the material into the extruder (3), the polymers were melted and homogeneously mixed with the powder by the two co-rotating screws.

**Figure 5.** Schematic extrusion process.

The screws transport the material to the extrusion nozzle (4), where the melted feedstock is forced through. The extrusion die has a bread-shaped opening to produce strands of this geometry, as shown in Figure 6a. This shape was chosen because bread-shaped magnets are preferred for electric rotor arrangements.

Figure 6b shows a comparison between the green and sintered parts, with the sintered part exhibiting approximately 20% shrinkage. Additionally, Figure 6c shows a plan view of the extruded green part.

The haul-off belt (5) continuously pulls the strand out of the die at a pre-set speed. To prevent oxidation of the raw material and the extruded strand, the entire compounding and extrusion process was carried out in an argon atmosphere with an argon-flushed glove box. The barrel in which the screws rotated was divided into six heating zones. The extrusion parameters used for the tests are shown in Table 5.

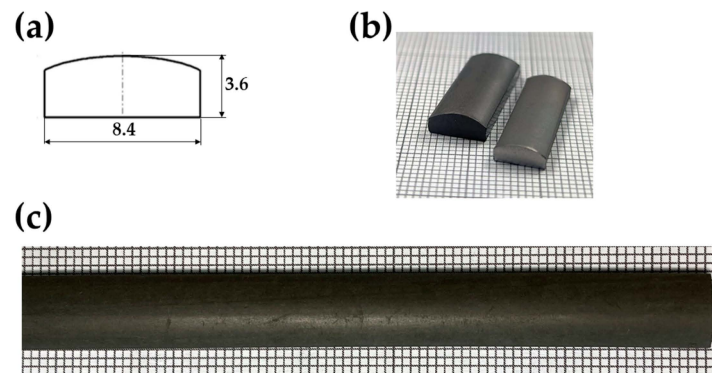


Figure 6. (a) Bread-shaped cross section, (b) cut green part and sintered part, (c) extruded strand green part.

The correct dosing of the coated powder and the backbone binder is crucial to homogeneous green part production. The nominal output parameters of the feeders must be matched to the extruder screw and take-off belt speeds. The profile’s stability depends on the haul-off speed. If the take-off speed is too high, the strand will become thinner; if the haul-off speed is too low, the melt will swell after leaving the die.

The extrusion die is shown in more detail in Figure 7a,b. The compound feedstock is forced under pressure through a bread-shaped die (3) to form a continuous strand. As seen in Figure 7a, the extrusion die must be fed through an inlet (4) in the glove box, implying that the melt must travel a long distance from the extruder (5) to the die. Therefore, an additional heating element (2) is required in front of the extrusion die. The extrusion die is fixed to the heated zone with a retaining ring and heated in this way.

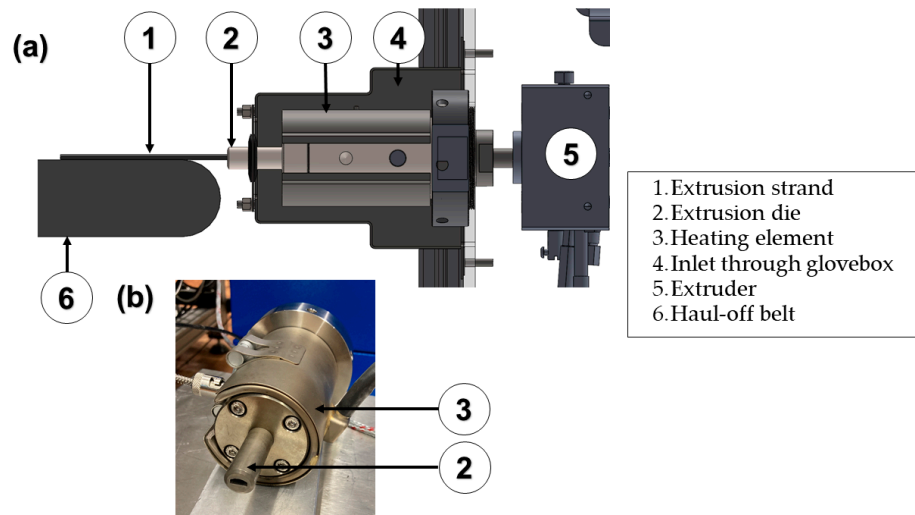


Figure 7. (a) Extrusion die side view of the CAD model, (b) Extrusion die with heating element.

2.3. Debinding and Sintering

The samples in this study were debinded and sintered by SUSMAGPRO project partner MIMplus Technologies GmbH & Co.KG in Ispringen, Germany.

3. Results and Discussion

3.1. Dimension Stability of the Extruded Green Parts

Feedstocks A, B, and C were extruded at different parameters. The deviations from the cross-sectional geometry of the green part were measured over a length of 500 mm at 10 measuring points. The reference width is 8.4 mm, and the reference height is 3.6 mm. Figure 8 shows the measuring points of feedstock A with different parameters.

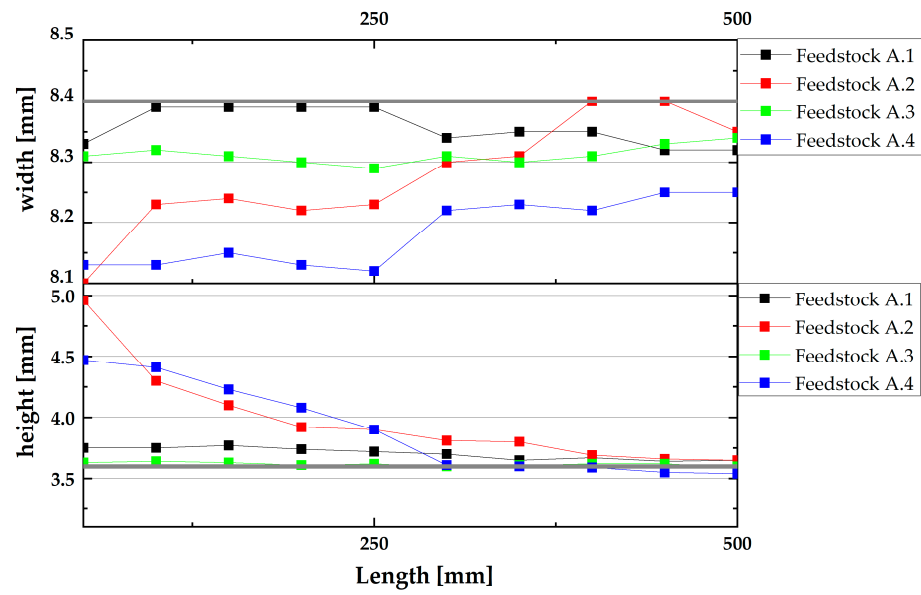


Figure 8. Dimensions stability of feedstock A.

In the variants extruded at 15 rpm (A2, A4), the melt sagged after leaving the die, resulting in a thinning of the width and an increase in the height of the part. This effect was minimised by increasing the haul-off speed from 0.15 m/min to 0.2 m/min. Extruded at a slower screw speed, extrudates A1 and A3 exhibited constant values over the entire length. Sample A achieved the most constant dimensional stability with 60 vol% powder loading. Feedstock B showed constant dimensional stability for all parameters. The feedstock with slow screw speed and 60 vol% powder loading showed only a small change in cross-section. These cross-sectional changes are shown in Figure 9.

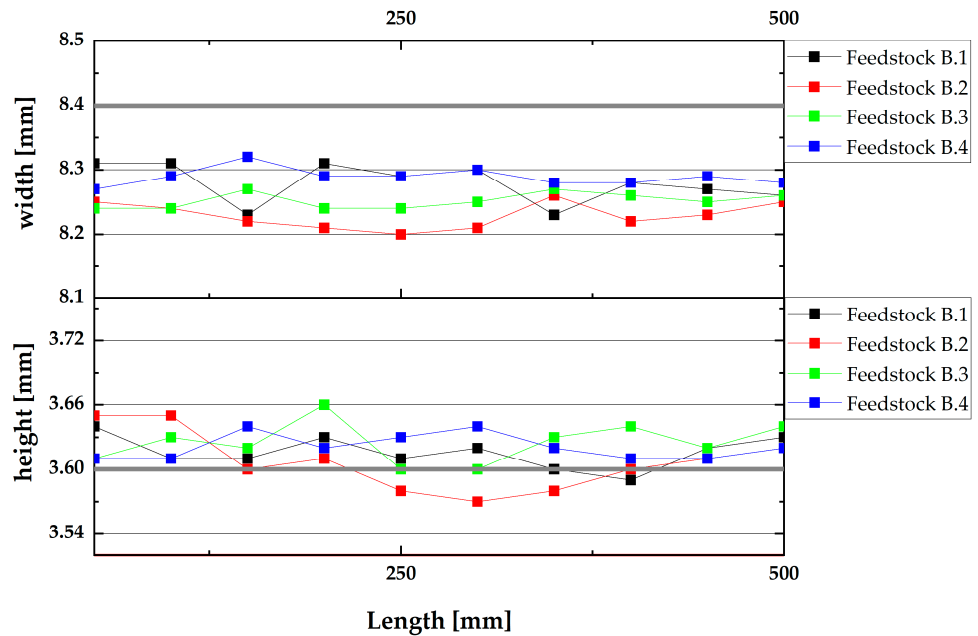


Figure 9. Dimensions stability of feedstock B.

The distribution of feedstock C is similar to feedstock A, as shown in Figure 10. By adjusting the haul-off speed, an approximation to the reference dimensions was achieved. Again, the 7 rpm variants were more geometrically stable over 500 mm.

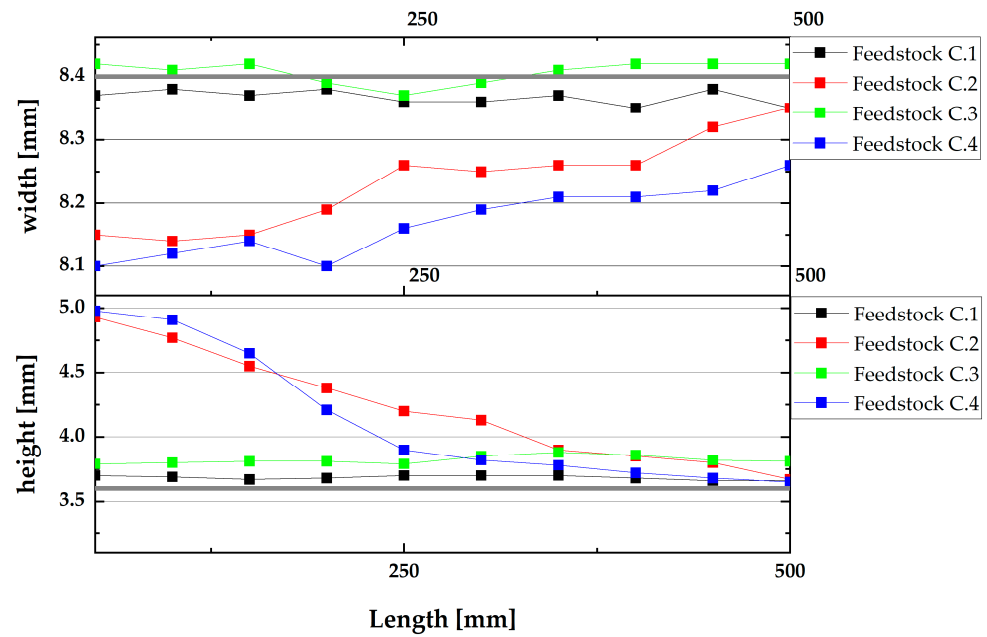


Figure 10. Dimensions stability of feedstock C.

Powder loading does not appear to affect the stability of the geometry. For feedstocks A and C, the 50 vol% and 60 vol% variants have the same sag after exiting the nozzle at 15 rpm. At slower speeds, the 50 vol% and 60 vol% strands also showed similar values. The three selected feedstock variables showed no differences in extrusion strand dimensional stability. These results were expected as the feedstock variants only differ in the amount of NdH_{2.7} added and whether they are non-degassed or degassed.

3.2. Carbon and Oxygen Content of Sintered Parts

Oxygen values were measured using the hot gas extraction method. Carbon levels were measured at Pforzheim University using a CS744 carbon analyser from Leco Instrumente GmbH (Mönchengladbach, Germany). The measurements are shown in Figure 11.

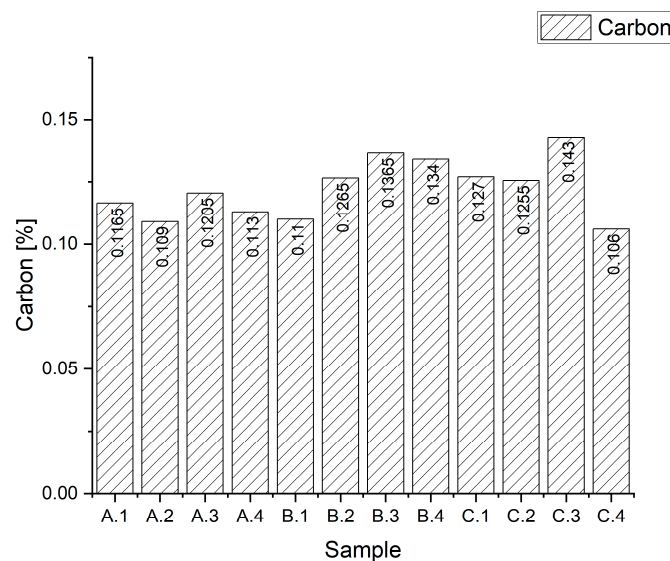


Figure 11. Carbon values of sintered samples.

For feedstock A, samples with 50 vol% powder loading have a slightly higher carbon value than samples with 60 vol%. Samples A.1 and A.3 have about 0.11 wt% carbon and

samples A.2 and A.4 have about 0.1 wt% carbon. For feedstock B, the two samples with 50 vol% powder loading show different values. Sample B.1 has a carbon content of 0.11 wt% and sample B.2 has a carbon content of 0.127 wt%. Samples with 60 vol% powder loading have 0.135 wt% carbon. Feedstock C also shows differences at 50 vol% powder loading. Sample C.3 with 0.143 wt% has a significantly higher carbon content than sample C1 with 0.126 wt%. Sample C.4 has the best carbon value of all samples at 0.10 wt%. Carbon values are just at the limit for good coercivity values, averaging over 0.11 wt%, as according to Lopes et al. [23], a drop in coercivity occurs between 0.095 wt% and 0.15 wt%.

The oxygen content of samples A.1–A.4 is about 0.8 wt%. Sample set B shows a greater variation in oxygen content. Samples B.2 (0.85 wt%) and B.4 (0.95 wt%) have a higher oxygen content than samples B.1 and B.3 with 0.75 wt% each. Feedstock C oxygen content is about 0.8 wt% for all four samples, similar to feedstock A. Oxygen values with an average of 0.8 wt% are within the limit defined by Minowa et al. [24] and Kim et al. [25], indicating that the process can produce magnets with high $BH_{(max)}$ values. As there were no oxygen values obtainable from the original magnet, this study relied on literature values from magnets produced through the MIM technique with recycled material. Kukla et al. [15] produced samples from recycled NdFeB material using the MIM process and achieved oxygen values of 0.72 wt%, indicating an approximate increase of 0.04 wt% in the production process. The oxygen value of output material by Burkhardt et al. [22] was 0.4–0.6 wt%.

These values indicate that slight oxygen uptake occurs during the applied process, as summarised in Figure 12. The produced samples showed good coercivity values, except samples A.3 and A.4 (Table 6). Since no traces of α -iron were found in the samples' microstructure, it can be assumed that the oxygen values were acceptable.

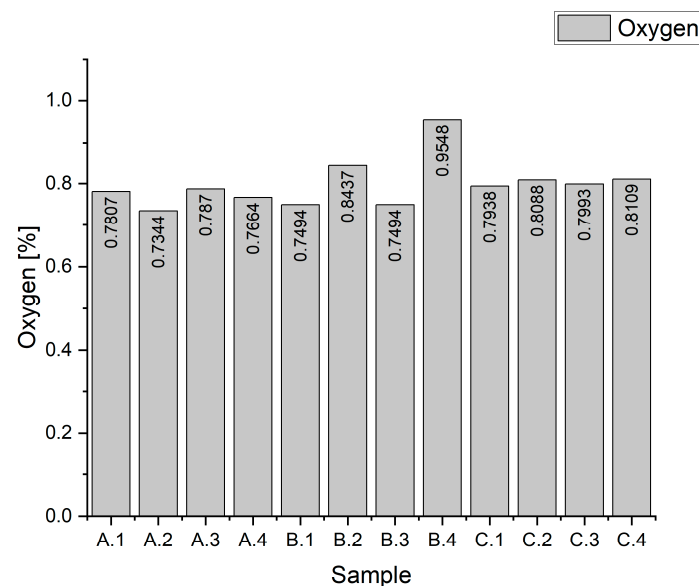


Figure 12. Oxygen values of sintered samples.

3.3. Magnetic Characterisation of the Sintered Parts

The sintered parts were magnetised after sintering using a K-series pulse magnetiser from Magnet Physik Dr. Steingroever GmbH (Cologne, Germany). The magnet was pulsed once and set to the highest value, 2000 V. The magnetic properties were measured with the Hystograph HG200 from Dr. Brockhaus Messtechnik GmbH & Co. KG (Lüdenscheid, Germany). Density was measured using the Archimedean principle. The measurement results are provided in Table 6. Sample B.4 was excluded from the measurements as its low density of 6.06 g/cm^3 did not allow feasible magnetic properties measurement.

Samples A.3 and A.4 (with 1 wt% $\text{NdH}_{-2.7}$ addition) exhibited the lowest coercivity iH_C of about 1000 kA/m. The coercivity iH_C of samples B and C (with 3 wt% $\text{NdH}_{-2.7}$ added) was between 1300 kA/m and 1500 kA/m. There was a correlation between magnetic

properties and the amount of NdH_{2.7} added. On average, lower values of the coercivity H_c were measured at 1 wt% NdH_{2.7} addition than at 3 wt% NdH_{2.7} addition. NdH_{2.7} additions did not affect the B_r remanence measurement due to the low overall remanence of the unaligned samples.

Table 6. Magnetic values and density.

| Sample | H_c (kA/m) | B_r (mT) | Density [g/cm ³] |
|--------|--------------|------------|------------------------------|
| A.1 | 1123 | 511 | 7.21 |
| A.2 | 1270 | 531 | 7.28 |
| A.3 | 956 | 555 | 7.20 |
| A.4 | 1053 | 539 | 7.21 |
| B.1 | 1429 | 531 | 7.23 |
| B.2 | 1353 | 547 | 7.23 |
| B.3 | 1137 | 534 | 7.15 |
| B.4 | - | - | 6.06 |
| C.1 | 1344 | 496 | 7.20 |
| C.2 | 1237 | 516 | 7.22 |
| C.3 | 1301 | 500 | 7.22 |
| C.4 | 1506 | 478 | 7.15 |

The degassed powder showed slightly lower B_r remanence values than the degassed powder, indicating that all hydrogen was removed during the final sintering step and that the hydrated powder may have had a lower oxygen uptake. However, this observation must be confirmed with systematic O measurements during all processing steps.

There was no difference in the magnetic properties of the three feedstock variants, neither with the 50 vol% or 60 vol% powder fillings. The density was also balanced for all samples, except for sample B.4. The powder filling did not influence the geometry during extrusion. With a remanence ranging from 500 mT to 555 mT, the samples exhibited the standard properties of isotropic NdFeB magnets. Compared to the reference values of isotropic MIM magnets produced from recycled material, the magnetic properties of magnets produced with PEM were similar. Kukla et al. [15] produced MIM magnets with 570 mT remanence. Similarly, Burkhardt et al. [22] produced isotropic MIM magnets with remanence values ranging from 560 mT to 580 mT.

3.4. Microstructure of the Sintered Parts

SEM images were captured with a Flex SEM 1000 of Hitachi High-Tech GmbH (Krefeld, Germany) at Pforzheim University.

Figures 13–15 show the microstructure of samples A.2, B.1, and C.4 in the centre and left edge zones of the section. These samples exhibit the best magnetic properties of the respective feedstock materials and were further investigated. The micrographs of the other samples are shown in Appendix A. The samples show a fine-grained microstructure with a uniform distribution of hard-magnetic Nd₂Fe₁₄B and Nd-rich phases.

The microstructure of sample A.1 showed only a few small pores of about 5 μ m, resulting in a fairly good density of 7.28 g/m³. It should be noted that some of the visible pores were the effects of sample preparation, as oxidised NdH_{2.7} can detach from the magnet surface during polishing. Sample B.1 had significantly more pores than sample A.2. The pores in sample B.1 were about 50 μ m in size and were evenly distributed in the cross-section of the sample. The pores in sample C.4 were significantly larger and deeper than samples A.2 and B.1. The microstructure in Figure 15 reveals a pore of approximately 200 μ m in length. Although the pores are larger, they are less distributed than in sample B.1 and still result in reduced density compared to the other samples. According to the micrographs, both screw speeds resulted in well-homogenised starting materials, uniformly distributed Nd-rich phases, and good density values. All micrographs show that the typical microstructure of sintered NdFeB magnets produced by the MIM process is comparable to that of conventional sintered NdFeB-type magnets [15,22]. The average density of the

samples was 7.2 g/cm^3 , which is lower than the 7.45 g/cm^3 of the original magnet; however, the developed PEM process still produced promising magnetisation values.

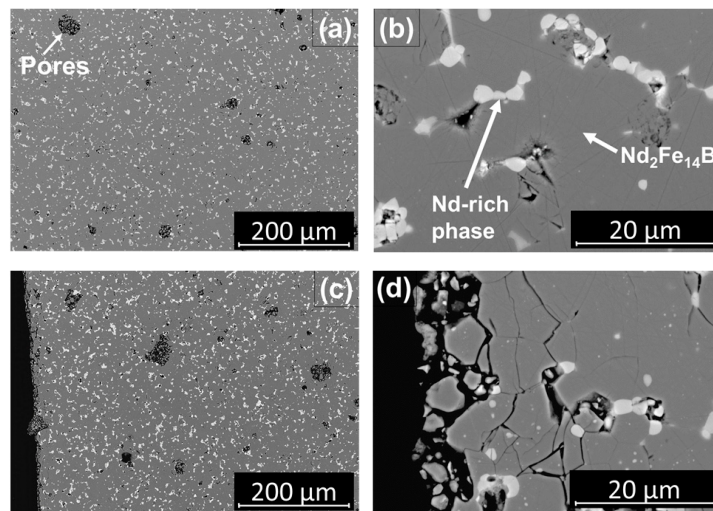


Figure 13. SEM observation of sample A.2: middle zone (a,b) and left edge (c,d).

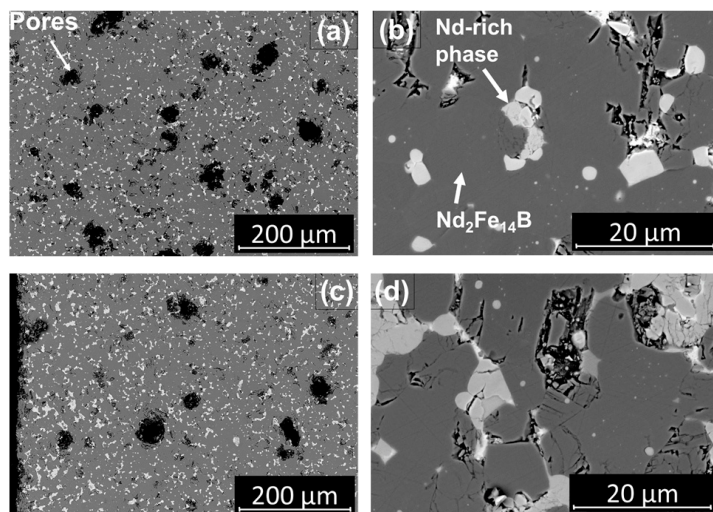


Figure 14. SEM observation of sample B.1: middle zone (a,b) and left edge (c,d).

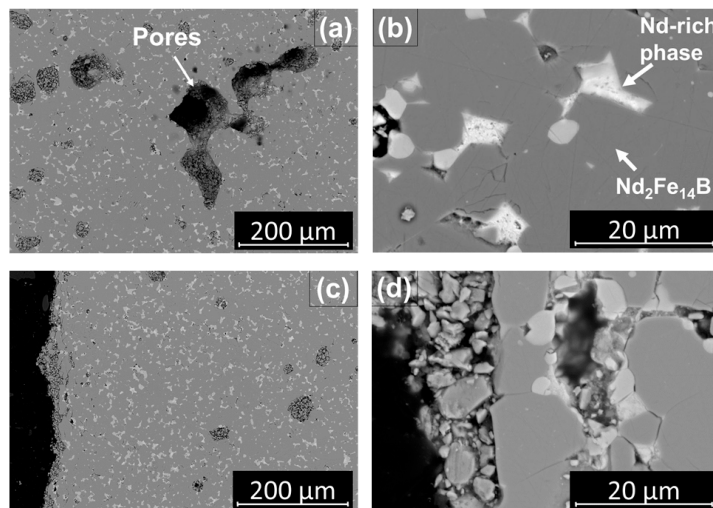


Figure 15. SEM observation of sample C.4: middle zone (a,b) and left edge (c,d).

4. Summary/Further Work

The objective of this study was to demonstrate the feasibility of producing NdFeB permanent magnets using the PEM process. Extrusion tests were carried out using different process parameters and material variants. This study investigated the extrusion conditions required to produce a strand of stable geometry and microstructure. The results showed that screw speeds of 7 rpm produced consistently more stable cross-sections over a length of 500 mm compared to a faster screw speed of 15 rpm. The strands showed almost no difference in geometric stability at powder fillings of 50 vol% and 60 vol%.

Oxygen and carbon values are crucial to NdFeB permanent magnet production. The measured carbon and oxygen values were in an acceptable range, as the samples showed no signs of α -iron in the micrographs. The measured magnetic properties were also comparable with the literature, as described in Section 3, “Carbon and Oxygen content of the sintered parts”.

Overall, samples containing 3 wt% NdH_{2.7} exhibited the best magnetic properties.

The next steps include systematic measurement of O, H, and C values in each production step and implementing an alignment tool to create anisotropic permanent magnets.

Author Contributions: Conceptualization, S.R., S.S. and C.B.; formal analysis, S.R., C.K. and C.B.; funding acquisition, C.B.; investigation, S.R.; methodology, S.R., S.S. and C.B.; project administration, S.R., C.K. and C.B.; resources, C.H. and C.B.; supervision, C.K., C.H. and C.B.; validation, S.R. and C.B.; visualization, S.R., C.K. and C.B.; writing—original draft, S.R.; writing—review and editing, S.R., C.K. and C.B. All authors have read and agreed to the published version of the manuscript.

Funding: This research was carried out as part of the SUSMAGPRO project funded by the European Union’s Horizon 2020 research and innovation programme under Grant Agreement No. 821114.

Data Availability Statement: The data presented in this study are available upon request from the corresponding author.

Acknowledgments: The authors would like to thank Laura Grau from the Institute for Precious and Technology Metals at Pforzheim University for providing Figure 2.

Conflicts of Interest: The authors declare no conflicts of interest. The funders had no role in the design of the study; in the collection, analyses, or interpretation of data; in the writing of the manuscript, or in the decision to publish the results.

Appendix A. Microstructures of Sample A1–C3

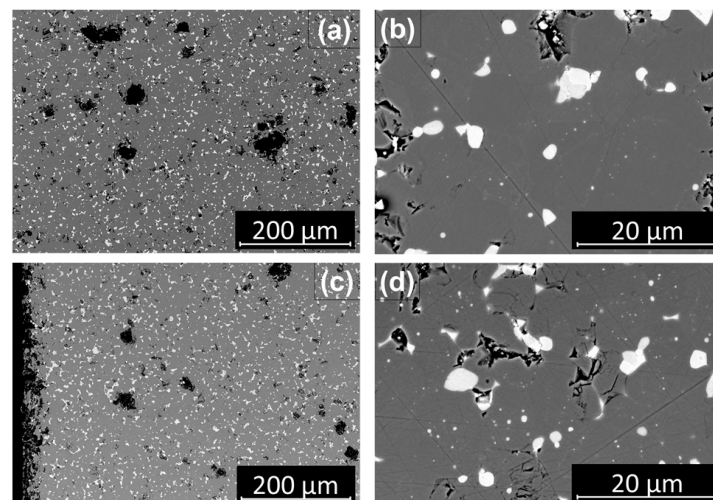


Figure A1. SEM observation of sample A.1: middle zone (a,b) and left edge (c,d).

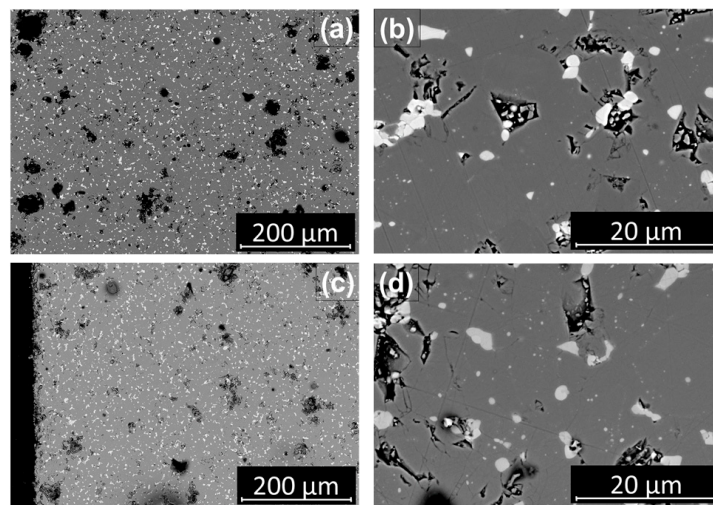


Figure A2. SEM observation of sample A.3: middle zone (a,b) and left edge (c,d).

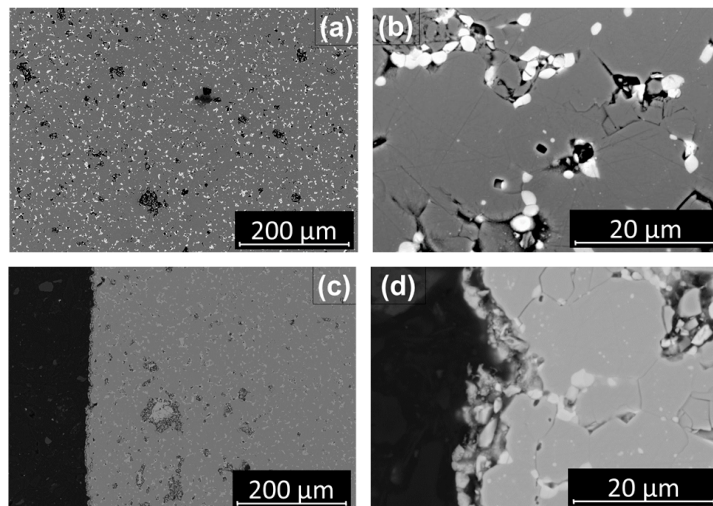


Figure A3. SEM observation of sample A.4: middle zone (a,b) and left edge (c,d).

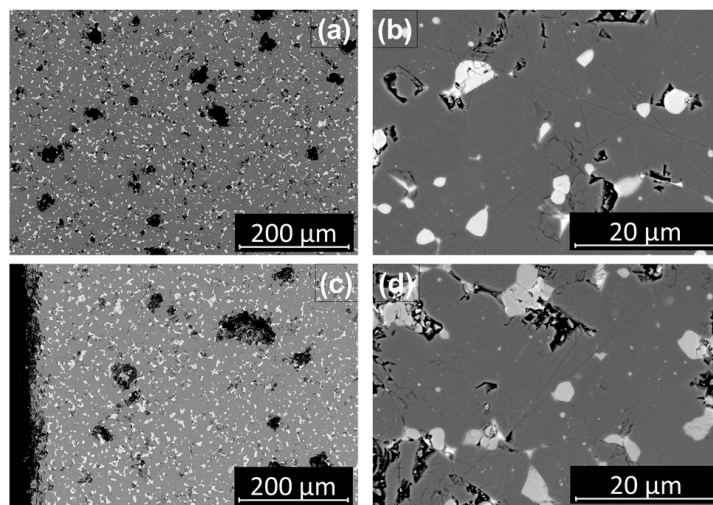


Figure A4. SEM observation of sample B.2: middle zone (a,b) and left edge (c,d).

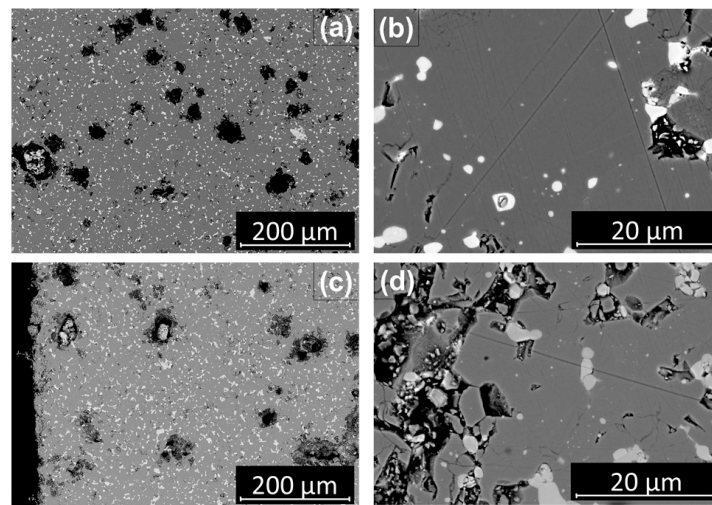


Figure A5. SEM observation of sample B.3: middle zone (a,b) and left edge (c,d).

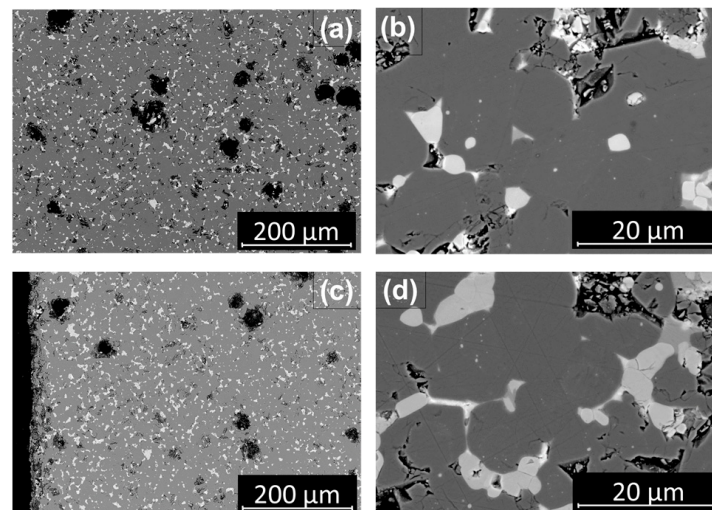


Figure A6. SEM observation of sample C.1: middle zone (a,b) and left edge (c,d).

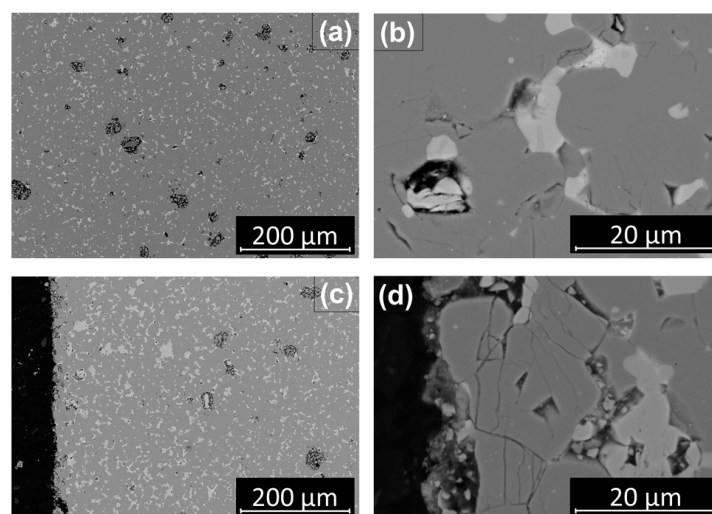


Figure A7. SEM observation of sample C.2: middle zone (a,b) and left edge (c,d).

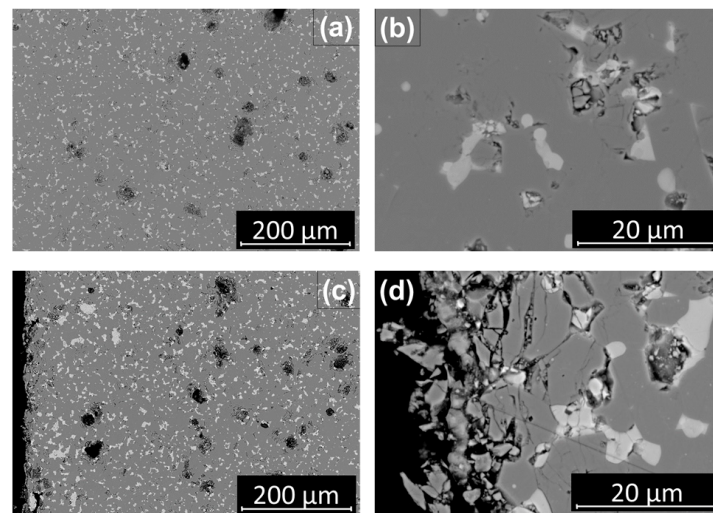


Figure A8. SEM observation of sample C.3: middle zone (a,b) and left edge (c,d).

References

1. European Commission and Directorate-General for Communication. *European Critical Raw Materials Act*; Publications Office of the European Union: Luxembourg, 2023. [CrossRef]
2. Gauß, R.; Burkhardt, C.; Carencotte, F.; Gasparon, M.; Gutfleisch, O.; Higgins, I.; Karajić, M.; Klossek, A.; Mäkinen, M.; Schäfer, B.; et al. *Rare Earth Magnets and Motors: A European Call for Action*; A Report by the Rare Earth Magnets and Motors Cluster of the European Raw Materials Alliance; European Raw Materials Alliance (ERMA): Berlin, Germany, 2021. Available online: <https://erma.eu/european-call-for-action/> (accessed on 14 April 2024).
3. Homepage Cordis European Commission, Horizon 2020. Sustainable Recovery, Reprocessing and Reuse of Rare-Earth Magnets in a Circular Economy (SUSMAGPRO). Grant agreement ID: 821114. Available online: <https://cordis.europa.eu/project/id/821114> (accessed on 14 April 2024).
4. Crozier-Bioud, T.; Momeni, V.; Gonzalez-Gutierrez, J.; Kukla, C.; Luca, S.; Rolere, S. Current challenges in NdFeB permanent magnets manufacturing by Powder Injection Molding (PIM): A review. *Mater. Today Phys.* **2023**, *34*, 101082. [CrossRef]
5. Ma, B.; Herchenroeder, J.; Smith, B.; Suda, M.; Brown, D.; Chen, Z. Recent development in bonded NdFeB magnets. *J. Magn. Mater.* **2002**, *239*, 418–423. [CrossRef]
6. Schatt, W.; Wieters, K.-P.; Kieback, B. (Eds.) *Pulvermetallurgie. Technologien und Werkstoffe, 2., Bearb. Und Erw. Aufl. 2007*; Springer: Berlin/Heidelberg, Germany, 2006.
7. Rodewald, W.; Katter, M.; Reppe, G. Fortschritte bei pulvermetallurgisch hergestellten Neodym-Eisen-Bor Magneten. In Proceedings of the Hager Symposium Pulvermetallurgie, Hagen, Germany, 28–29 September 2002.
8. Sagawa, M.; Fujimura, S.; Togawa, N.; Yamamoto, H.; Matsuura, Y. New material for permanent magnets on a base of Nd and Fe (invited). *J. Appl. Phys.* **1984**, *55*, 2083–2087. [CrossRef]
9. Hadjipanayis, G.C. (Ed.) Bonded Magnets. In Proceedings of the NATO Advanced Research Workshop on Science and Technology of Bonded Magnets, Newark, NJ, USA, 22–25 August 2002; Springer: Dordrecht, The Netherlands, 2003.
10. Cheng, X.; Yu, X. Effect of Binder and Additives on Properties of NdFeB Bonded Magnets by Injection Moulding. *J. Iron Steel Res. Int.* **2006**, *13*, 282–285. [CrossRef]
11. Beiss, P. *Pulvermetallurgische Fertigungstechnik*; Springer: Berlin/Heidelberg, Germany, 2013.
12. Klocke, F. *Fertigungsverfahren 5*; Springer: Berlin/Heidelberg, Germany, 2018.
13. Gonzalez-Gutierrez, J.; Stringari, G.; Emri, I. Powder Injection Molding of Metal and Ceramic Parts. In *Some Critical Issues for Injection Molding*, 1st ed.; Wang, J., Ed.; Article 3; INTECH: Houston, TX, USA, 2012; pp. 65–88. [CrossRef]
14. European Powder Metallurgy Association (EPMA). *Introduction to Metal Injection Moulding Technology. A Manufacturing Process for Precision Engineering Components*, 4th ed.; European Powder Metallurgy Association (EPMA): Shrewsbury, UK, 2017.
15. Kukla, C.; Imgrund, P.; Weber, O.; Schlauf, T.; Pickering, L.; Pischang, K.; Walton, A.; Gonzalez-Gutierrez, J.; Burkhardt, C. Metal Injection Moulding of NdFeB Based on Recycled Powders. In Proceedings of the World PM 2016 Congress and Exhibition, Hamburg, Germany, 9–13 October 2016.
16. Lopes, L.U.; Hartwig, T.; Wendhausen, P.A.P. Evaluation of Process Variables in the Alignment Factor of Nd-Fe-B Magnets Made by Metal Injection Molding. *IEEE Trans. Magn.* **2013**, *49*, 4618–4621. [CrossRef]
17. Hartwig, T.; Lopes, L.; Wendhausen, P.; Ünal, N. Metal Injection Molding (MIM) of NdFeB Magnets. *EPJ Web Conf.* **2014**, *75*, 4002. [CrossRef]
18. Gonzalez-Gutierrez, J.; Thompson, Y.; Handl, D.; Cano, S.; Schuschnigg, S.; Felfer, P.; Kukla, C.; Holzer, C.; Burkhardt, C. Powder content in powder extrusion moulding of tool steel: Dimensional stability, shrinkage and hardness. *Mater. Lett.* **2021**, *283*, 128909. [CrossRef]

19. Sotomayor, M.; Levenfeld, B.; Varez, A. Powder extrusion moulding of 430L stainless steel thin tubes for porous metal supported SOFCs. *Powder Metall.* **2011**, *54*, 103–107. [[CrossRef](#)]
20. Banerjee, S.; Joens, C.H. Debinding and sintering of metal injection molding (MIM) components. In *Handbook of Metal Injection Molding*; Woodhead Publishing: Cambridge, UK; Philadelphia, PA, USA, 2012.
21. Davies, B.; Mottram, R.; Harris, I. Recent developments in the sintering of NdFeB. *Mater. Chem. Phys.* **2002**, *67*, 272–281. [[CrossRef](#)]
22. Burkhardt, C.; Weber, O.; Podmiljsak, B.; Gonzalez-Gutierrez, J.; Kukla, C.; Degri, M.; Harris, I.; Walton, A. Isotropic NdFeB hard magnets: MIM production using recycled powders with and without Nd additions. *Powder Inject. Mould. Int.* **2017**, *11*, 75–81.
23. Lopes, L.U.; Santos, E.C.; Hartwig, T.; Wendhausen, P.A. Investigation of the influence of carbon on the magnetic properties of powder injection molded Nd-Fe-B magnet. In Proceedings of the 2015 IEEE International Magnetics Conference (INTERMAG), Beijing, China, 11–15 May 2015; p. 1.
24. Minowa, T.; Shima, M.; Honshima, M. Microstructure of Nd-rich phase in Nd-Fe-B magnet containing oxygen and carbon impurities. *J. Magn. Magn. Mater.* **1991**, *97*, 107–111. [[CrossRef](#)]
25. Kim, A.S. Effect of oxygen on magnetic properties of Nd-Fe-B magnets. *J. Appl. Phys.* **1988**, *64*, 5571–5573. [[CrossRef](#)]
26. Walton, A.; Yi, H.; Rowson, N.A.; Speight, J.D.; Mann, V.; Sheridan, R.S.; Bradshaw, A.; Harris, I.R.; Williams, A.J. The use of hydrogen to separate and recycle neodymium–iron–boron-type magnets from electronic waste. *J. Clean. Prod.* **2015**, *104*, 236–241. [[CrossRef](#)]
27. Sprecher, B.; Kleijn, R.; Kramer, G.J. Recycling potential of neodymium: The case of computer hard disk drives. *Environ. Sci. Technol.* **2014**, *48*, 9506–9513. [[CrossRef](#)] [[PubMed](#)]
28. Yang, Y.; Walton, A.; Sheridan, R.; Güth, K.; Gauß, R.; Gutfleisch, O.; Buchert, M.; Steenari, B.-M.; van Gerven, T.; Jones, P.T.; et al. REE Recovery from End-of-Life NdFeB Permanent Magnet Scrap: A Critical Review. *J. Sustain. Metall.* **2017**, *3*, 122–149. [[CrossRef](#)]
29. Zakotnik, M.; Devlin, E.; Harris, I.R.; Williams, A. Hydrogen Decrepitation and Recycling of NdFeB-type Sintered Magnets. *J. Iron Steel Res. Int.* **2006**, *13*, 289–295. [[CrossRef](#)]
30. Thomas, B.; Maelig, O.; Loïc, F.; Sorana, L.; Sébastien, R. Net-Shaped NdFeB Magnets Made By Powder Injection Molding: Lowering The Organic Contamination. In Proceedings of the World PM 2022 Congress and Exhibiton, Lyon, France, 9–13 October 2022; Session 68: Functional Materials Hard Magnetics.
31. Tang, W.; Ouyang, G.; Cui, B.; Wang, J.; Dennis, K.W.; Kramer, M.J.; Anderson, I.E.; Cui, J. Magnetic and mechanical properties of grain-refined Dy-free Nd-Fe-B sintered magnets. *J. Magn. Magn. Mater.* **2021**, *521*, 167533. [[CrossRef](#)]
32. Mottram, R.; Davis, B.; Yartys, V.; Harris, I. The use of metal hydride powder blending in the production of NdFeB-type magnets. *Int. J. Hydrogen Energy* **2001**, *26*, 441–448. [[CrossRef](#)]
33. Bonten, C. Kunststofftechnik. In *Einführung und GrundlagenMünchen*; Carl Hanser Verlag GmbH & Co. KG: Munich, Germany, 2014.

Disclaimer/Publisher’s Note: The statements, opinions and data contained in all publications are solely those of the individual author(s) and contributor(s) and not of MDPI and/or the editor(s). MDPI and/or the editor(s) disclaim responsibility for any injury to people or property resulting from any ideas, methods, instructions or products referred to in the content.